ELSEVIER

Journal of Magnetism and Magnetic Materials 200 (1999) 439–455

Journal of magnetism and magnetic materials

www.elsevier.com/locate/jmmm

Stress and magnetic properties of surfaces and ultrathin films

D. Sander*, A. Enders, J. Kirschner

Max-Planck-Institut für Mikrostrukturphysik, Weinberg 2, D-06120 Halle, Germany

Received 22 January 1999

Abstract

Stress measurements with sub-monolayer sensitivity are performed to investigate the correlation between mechanical film stress and magneto-elastic anisotropy in epitaxial ferromagnetic monolayers. The magneto-elastic coupling B_1 of Fe(1 0 0) films is measured directly. Magnitude and sign of B_1 deviate from the respective bulk value. A strain-dependent correction of the magneto-elastic coupling coefficient B_1 describes the apparent thickness dependence of B_1 for film thicker than 10 nm. For thinner films, the possible contribution of surface corrections is discussed to explain the almost constant B_1. The implications of a modified magneto-elastic coupling for the anisotropy of ultrathin films is elucidated.

Keywords: Stress; Surfaces; Thin films; Monolayers; Anisotropy

1. Introduction

The magneto-elastic properties of ultrathin films or of bulk samples within a few Å near the sample surface have been reported to differ substantially from the respective bulk properties. Sun and O'Handley found that the magneto-elastic coupling can differ by more than a factor of three near the surface region of amorphous alloys [1]. Szymczak and Żuberek measured that the magnetostriction of Ni/Pb and Ni/C multilayers is proportional to the inverse Ni layer thickness, and they ascribed their findings to a surface magnetostriction contribution [2]. Others found that the application of a mechanical stress to a ferromagnetic bulk sample changed the magnitude of the saturation magnetostriction [3,4]. Recently, Koch et al. described a linear correlation between film stress and the magnitude of the effective magneto-elastic coupling coefficient, that leads to change of sign of the magneto-elastic coupling in strained Fe(1 0 0) films [5]. Finally, Kim and Silva reported that the magnetostriction of permalloy, a material with negligible magnetostriction as a bulk sample, raises to significant values for permalloy films thinner than 10 nm [6]. All these examples indicated that one should not be too surprised to find that magnitude and sign of the magneto-elastic coupling coefficients differ substantially from their respective bulk values in the case of *ultrathin* and *strained* ferromagnetic films.

* Corresponding author. Tel.: + 49-345-5582-660; fax: + 49-345-5511-223.
E-mail address: sander@mpi-halle.mpg.de (D. Sander)

0304-8853/99/$ - see front matter
PII: S0304-8853(99)00310-8

Table 1
Anisotropy constants K_i, magneto-elastic coupling coefficients B_i, calculated from λ_i (see Table 2), and stray field energy density $\mu_0 M_S^2/2$. Room temperature values from Ref. [19] in MJ/m^3

	BCC Fe	FCC Ni	HCP Co
K_1	0.048	− 0.006	0.513
K_2	0.0001	− 0.003	0.013
B_1	− 3.43	9.38	− 8.1
B_2	7.83	10	− 29
B_3			28.2
B_4			29.4
$\mu_0 M_S^2/2$	1.85	0.15	1.32

It is the goal of this contributions to present experimental evidence for the intimate correlation between film stress and magnetic anisotropy in nm epitaxial films. Our results indicate that strain is an important factor for the modified magneto-elastic coupling in ultrathin films. Already moderate strains in the sub-percent range are found to induce a change of the sign of the magneto-elastic coupling coefficient of Fe(1 0 0) films. The implications for the magnetic anisotropy of strained epitaxial films are discussed.

2. Magneto-elastic coupling in epitaxial films

The magneto-elastic coupling describes strain-dependent contributions to the magnetic energy density f [7]. The magnitude of both film strain ε_i and magneto-elastic coupling coefficients B_j determine how film strain alters the magnetic anisotropy. For example, the magneto-elastic coupling coefficients in cubic systems are two to three orders of magnitude larger than the magneto-crystalline anisotropy constants, see Table 1, and even small strains in the sub-percent range are capable of modifying the magnetic anisotropy considerably. However, it is a doubtful practice to apply *bulk* magneto-elastic coupling coefficients to the discussion of magnetic anisotropy of ultrathin films as several recent experimental works proved that in sharp contrast to bulk behavior *magnitude and sign of the magneto-elastic coupling coefficients are not constant, but seem to vary with film thickness and film stress* [1,5,8]. The correlation between film stress measurements with magnetostrictive bending experiments [9,10], that are explained in the next section, corroborated the decisive role of film strain for the modified magneto-elastic behavior of nm thin films. We present results on the strain-dependent correction of the bulk value of B_1 in Section 5. It is found that strains larger than 0.6% induce a change of sign of B_1 in nm Fe(1 0 0) films [8]. In the following, the contributions of the magneto-crystalline anisotropy f_{mc} and of the magneto-elastic anisotropy f_{me} are compiled for various epitaxial film orientations to facilitate the discussion of magnetic anisotropy.

Starting point in a phenomenological description of the magnetic anisotropy f is the separation of the contribution of the magneto-crystalline anisotropy f_{mc}, the magneto-elastic anisotropy f_{me} and of the stray field energy density f_{demag}:

$$f(\alpha_i, \varepsilon_j) = f_{\mathrm{mc}}(\alpha_i) + f_{\mathrm{me}}(\alpha_i, \varepsilon_j) + f_{\mathrm{demag}}(\alpha_3). \tag{1}$$

The orientations of the magnetization direction is given by the direction cosines α_i, and the film strain is given by ε_j. The minimum of Eq. (1) gives the direction of the easy-axis of magnetization, differences between f for various orientations of the magnetization are calculated to derive in-plane and out-of-plane anisotropies. The following expressions for f_{mc} and f_{me} are used for cubic and hexagonal films [11]:

$$f_{\mathrm{mc}}^{\mathrm{cubic}} = K_1(\alpha_1^2\alpha_2^2 + \alpha_2^2\alpha_3^2 + \alpha_1^2\alpha_3^2) + \cdots, \tag{2}$$

Table 2
Relation between the B_i and the measured magnetostriction constants λ and the elastic constants c_{ij} for cubic and hexagonal systems

	Cubic [7]	Hexagonal [20]
B_1	$-\frac{3}{2}(c_{11}-c_{12})\lambda_{1\,0\,0}$	$-(c_{11}-c_{12})(\lambda_A-\lambda_B)$
B_2	$-3c_{44}\lambda_{1\,1\,1}$	$-c_{13}(\lambda_A+\lambda_B)-c_{33}\lambda_C$
B_3		$-c_{12}\lambda_A-c_{11}\lambda_B-c_{13}\lambda_C$
B_4		$c_{44}(\lambda_A+\lambda_B+\lambda_C-4\lambda_D)$

$$f_{mc}^{hex}=K_1\sin^2\phi+K_2\sin^4\phi+\cdots, \tag{3}$$

$$f_{me}^{cubic}=B_1(\varepsilon_1\alpha_1^2+\varepsilon_2\alpha_2^2+\varepsilon_3\alpha_3^2)+B_2(\varepsilon_4\alpha_2\alpha_3+\varepsilon_5\alpha_1\alpha_3+\varepsilon_6\alpha_1\alpha_2)+\cdots, \tag{4}$$

$$f_{me}^{hex}=B_1(\varepsilon_1\alpha_1^2+2\varepsilon_6\alpha_1\alpha_2+\varepsilon_2\alpha_2^2)+B_2(1-\alpha_3^2)\varepsilon_3+B_3(1-\alpha_3^2)(\varepsilon_1+\varepsilon_2)+B_4(\varepsilon_4\alpha_2\alpha_3+\varepsilon_5\alpha_1\alpha_3)+\cdots. \tag{5}$$

The magnetization direction is given by the α_i and the film strains are denoted ε_i, where the contracted Voigt-notation has been applied to contract the two-suffix symmetric strain tensor ε_{ij} to ε_k [12,13]. Both direction cosines α_i and strains ε_i are given in a cubic crystal system, which does *not* coincide with the film coordinate system in general. This requires appropriate tensor transformations for orientations other than cubic (1 0 0) or hexagonal (0 0 0 1). The necessary transformation is given as an example for the cubic (1 1 0) plane in Appendix A. The angle ϕ is measured between the c-axis and the magnetization direction. The dots indicate that higher-order terms in α_i are neglected. In the following we neglect even K_2, which is a reasonable assumption in the discussion of Fe, where K_2 is more than a factor of hundred smaller than K_1, see Table 2. Higher-order terms in ε_i are introduced later as a strain-dependent correction of B_1 [14]. The so-called surface terms that contribute in proportion to the inverse film thickness can be incorporated in the K_i [15,16] and B_i [2,17,18]. An example of a surface term K_S is presented below in the discussion of the in-plane anisotropy of Fe(1 1 0) monolayers. Values for K_i and B_i are given in Table 1. The demagnetizing field is zero for an in-plane magnetization of ultrathin films. The stray field energy density resulting from an out-of-plane magnetization is determined by the demagnetizing field and is given by the saturation magnetization M_S as

$$f_{demag}=\tfrac{1}{2}\mu_0 M_S^2.$$

Values of f_{demag} are quoted in Table 1.

Before we concentrate in the following on the in-plane anisotropy of Fe films with (1 0 0) and (1 1 0) surface orientations we compile the expressions for the magneto-crystalline and the magneto-elastic in-plane and out-of-plane anisotropies in Table 3. Table 3 quotes the in-plane and out-of-plane magnetic anisotropy as differences in energy density between two in-plane magnetization directions and between in-plane and out-of-plane magnetization, respectively. In the derivation of the expressions we considered isotropic film strain, $\varepsilon_1'=\varepsilon_2'=\varepsilon_0'$, the strain perpendicular to the film plane is given by ε_3', the primes indicate the film coordinate system. Table 3 shows that the magneto-elastic coupling affects the out-of-plane magnetic anisotropy for all film orientations. Therefore, an independent experimental determination of the B_i in the thickness and strain state of interest is of fundamental importance in the discussion of magneto-elastic strain effects. A procedure to measure B_i *directly* is presented in the next section. Whereas the in-plane strains are generally known from the epitaxial growth mode and the resulting misfit strain, or from a structural analysis by diffraction techniques [21], or from a stress analysis [13], the out-of-plane strain is often assumed to be given by continuum elasticity as a Poisson-type reaction of the in-plane strain. The following relations give the out-of-plane film strain ε_3' as a function of the isotropic in-plane strain ε_0' for various film orientations [13]:

$$\text{cubic (1 0 0):}\quad \varepsilon_3'=-\frac{c_{12}}{c_{11}}2\varepsilon_0', \tag{7}$$

Table 3
Magneto-crystalline anisotropy f_{mc} and magneto-elastic anisotropy f_{me}, calculated for an isotropic in-plane film strain ε'_0 and a perpendicular film strain ε'_3 for various epitaxial orientations. ε'_3 is alternatively expressed in terms of ε'_0, see Eqs. (7)–(10)

	f_{mc}	f_{me}
Cubic (1 0 0), in-plane, $f([1\,0\,0]) - f([1\,1\,0])$	$-\frac{1}{4}K_1$	0
Cubic (1 0 0), out-of-plane, $f([1\,0\,0]) - f([0\,0\,1])$	0	$B_1(\varepsilon'_0 - \varepsilon'_3)$
		$B_1\left(\frac{c_{11}+2c_{12}}{c_{11}}\varepsilon'_0\right)$
Cubic (1 1 0), in-plane, $f([0\,0\,1]) - f([\bar{1}\,1\,0])$	$-\frac{1}{4}K_1$	$\frac{1}{2}(B_1 - B_2)(\varepsilon'_0 - \varepsilon'_3)$
		$(B_1 - B_2)\left(\frac{c_{11}+2c_{12}}{c_{11}+c_{12}+2c_{44}}\right)\varepsilon'_0$
Cubic (1 1 0), out-of-plane, $f([\bar{1}\,1\,0]) - f([1\,1\,0])$	0	$B_2(\varepsilon'_0 - \varepsilon'_3)$
		$2B_2\left(\frac{c_{11}+2c_{12}}{c_{11}+c_{12}+2c_{44}}\right)\varepsilon'_0$
Cubic (1 1 1), in-plane, all directions	0	0
Cubic (1 1 1), out-of-plane, $f[-\frac{1}{\sqrt{2}}, \frac{1}{\sqrt{2}}, 0] - f[1\,1\,1]$	$-\frac{1}{12}K_1$	$B_2(\varepsilon'_0 - \varepsilon'_3)$
		$2B_2\left(\frac{c_{11}+2c_{12}-2c_{44}}{c_{11}+2c_{12}+4c_{44}}\right)\varepsilon'_0$
HCP (0 0 0 1), in-plane, all directions	0	0
HCP (0 0 0 1), out-of-plane	K_1	$(B_1 + 2B_3)\varepsilon'_0 + B_2\varepsilon'_3$
		$\left(B_1 + 2B_3 - \frac{2c_{13}}{c_{33}}B_2\right)\varepsilon'_0$

$$\text{cubic (1 1 0):}\quad \varepsilon'_3 = -\frac{c_{11}+3c_{12}-2c_{44}}{c_{11}+c_{12}+2c_{44}}\varepsilon'_0, \tag{8}$$

$$\text{cubic (1 1 1):}\quad \varepsilon'_3 = -\frac{c_{11}+2c_{12}-2c_{44}}{c_{11}+2c_{12}+4c_{44}}2\varepsilon'_0, \tag{9}$$

$$\text{HCP (0 0 0 1):}\quad \varepsilon'_3 = -\frac{c_{13}}{c_{33}}2\varepsilon'_0. \tag{10}$$

The elastic constants c_{ij} are given in Table 4.

Table 3 gives the difference in the energy density for two different orientations $f(1) - f(2)$ of the magnetization, a positive value indicates that the orientation (2) is energetically more favorable as it leads to a lower energy density. The stray field energy density f_{demag} has to be taken into account to decide whether the easy magnetization direction is out of plane.

The directional dependence of the magnetic anisotropy *within* the (1 1 0) plane of ultrathin Fe films on W(1 1 0) is of great interest as the so-called surface anisotropy contributions have been evoked to explain the easy in-plane magnetization direction along [$\bar{1}$ 1 0] [15,16], which deviates from the bulk Fe easy magnetization direction [1 0 0]. However, due to the large lattice misfit of more than 10% between Fe and W, film strain and its role in modifying the bulk magneto-elastic coupling [8,24] should not be ruled out as an alternative driving force for the reorientation of the easy magnetization axis from [1 0 0] to [$\bar{1}$ 1 0]. The role of a modified magneto-elastic coupling in Fe films for the magnetic anisotropy in (1 1 0) planes is discussed below.

Table 4
Elastic constants c_{ij} in GPa, values from Ref. [22,23]

	BCC Fe	FCC Ni	HCP Co
c_{11}	229	249	307
c_{12}	134	152	165
c_{44}	115	118	75.5
c_{13}			103
c_{33}			358

The in-plane magneto-crystalline anisotropy f_{mc} and the magneto-elastic anisotropy f_{me} are calculated for the cubic (1 0 0) and the cubic (1 1 0) planes. The results are plotted as polar plots in Fig. 1 for isotropic in-plane strains of $\varepsilon_0' = 0.01$. A strain of 1% is chosen as it leads to magneto-elastic anisotropy contributions that are comparable in magnitude with the magneto-crystalline anisotropy. Our in situ stress measurements suggest that 1% strain characterizes the average film strain in a 5 nm thin Fe(1 0 0) film on W(1 0 0).

The directional dependence of the magneto-crystalline and of the magneto-elastic anisotropy is given by

$$f_{\mathrm{mc}}^{(1\ 0\ 0)} = K_1(\cos^2(\alpha_1') - \cos^4(\alpha_1')), \tag{11}$$

$$f_{\mathrm{me}}^{(1\ 0\ 0)} = B_1\varepsilon_0'. \tag{12}$$

The magneto-crystalline anisotropy shows a fourfold symmetry, plotted in Fig. 1a. The lobes of the polar plot are extended along the [1 1 0] directions, indicative of a hard magnetization direction, the minima of the anisotropy are found in the [1 0 0] directions, as evidenced by the zero values of the anisotropy plot. The difference between the length of the radius vector at the lobe position versus the zero position gives the in-plane anisotropy of $K_1/4$, as quoted in Table 3. The magneto-elastic anisotropy contribution is isotropic and is represented by a dashed circle in Fig. 1b, the sum of both contributions is drawn as solid line in Fig. 1b. Note, that although the isotropic contribution inflates the anisotropy plot, the difference in length of the radius vector along two directions remains unchanged, indicating that an isotropic film strain does not change the in-plane anisotropy of an (1 0 0) film.

The situation is different for the (1 1 0) orientation. Here, the tensor transformations that are explained in Appendix A result in the following expressions for the angular dependence of the anisotropy contributions:

$$f_{\mathrm{mc}}^{(1\ 1\ 0)} = K_1(\cos^2(\alpha_1') - \tfrac{3}{4}\cos^4(\alpha_1')), \tag{13}$$

$$f_{\mathrm{me}}^{(1\ 1\ 0)} = \tfrac{1}{2}(B_2 - B_1)(\varepsilon_0' - \varepsilon_3')\cos^2(\alpha_1'). \tag{14}$$

Fig. 1c and Fig. 1d indicate that both magneto-crystalline anisotropy and magneto-elastic anisotropy favor an easy in-plane magnetization direction [0 0 1]. In sharp contrast to the (1 0 0) orientation, the magneto-elastic anisotropy leads to a large uniaxial anisotropy contribution, shown as a dashed curve in Fig. 1d, that is roughly a factor of five larger than the magneto-crystalline anisotropy. Consequently, the resulting sum of both anisotropy contributions is dominated by f_{me}, as indicated by the solid curve in Fig. 1d. However, this treatment fails to reproduce the easy magnetization direction along $[\bar{1}\ 1\ 0]$ that is experimentally observed for Fe films on W(1 1 0) in the thickness range 1–50 atomic layers ($\approx$10 nm) [15].

Elmers and Gradmann introduced in-plane surface anisotropy constants $K_{\mathrm{S,PP}}$ and $K_{\mathrm{S,P}}$ to take the effect of the broken symmetry at the film interface into account and proposed the following expressions for the magneto-crystalline anisotropy [16]:

$$f_{\mathrm{mc,S}}^{(1\ 1\ 0)} = \left(K_1 - \frac{K_{\mathrm{S,P}}}{d}\cos^2(\alpha_1')\right) + \left(-\frac{3}{4}K_1 - \frac{K_{\mathrm{S,PP}}}{d}\cos^4(\alpha_1')\right) \tag{15}$$

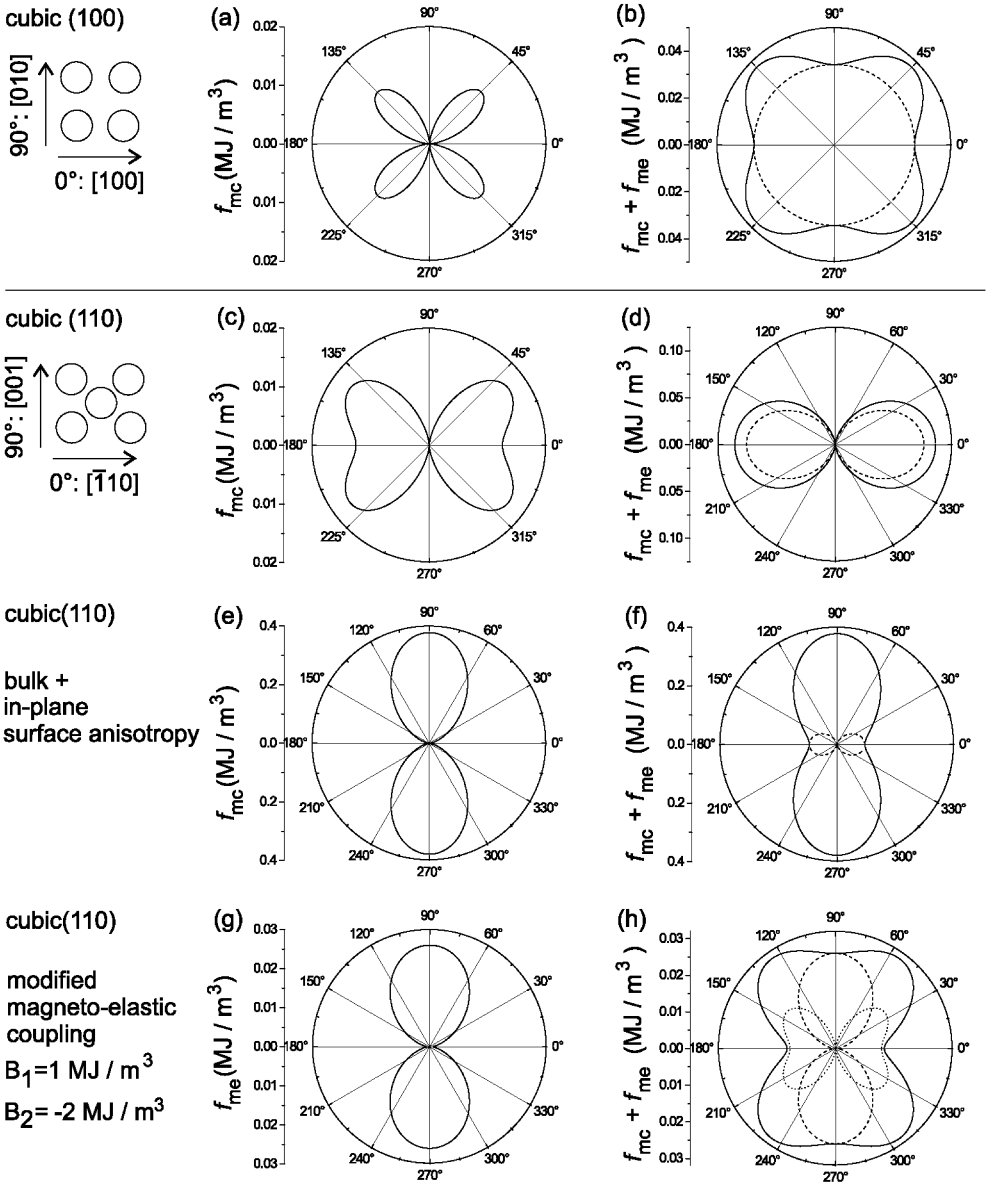

Fig. 1. Polar plots of the magneto-crystalline anisotropy f_{mc} and magneto-elastic anisotropy f_{me} of cubic (1 0 0) and (1 1 0) films. An isotropic in-plane strain of $\varepsilon_0' = 0.01$ is used in f_{me}. The length of the radius vector resembles the in-plane anisotropy. (b), (d), (f): dashed curve f_{me}, solid curve $f_{me} + f_{mc}$; (h): dashed curve f_{me}, dotted curve f_{mc}, solid curve $f_{me} + f_{mc}$.

with $K_{S,PP} = -0.16\ \mathrm{mJ/m^2}$, $K_{S,P} = 0.55\ \mathrm{mJ/m^2}$ and the film thickness given by d. This surface term correction leads to an easy magnetization direction along [$\bar{1}$ 1 0], as shown in Fig. 1e, plotted for $d = 1$ nm. With this surface term correction, the magneto-crystalline anisotropy is roughly a factor of six larger than the magneto-elastic anisotropy, that is shown as a dashed curve in Fig. 1f. The resulting sum of $f_{mc} + f_{me}$ is plotted as solid curve in Fig. 1f and indicates an easy in-plane magnetization direction along [$\bar{1}$ 1 0].

However, our experimental determination of B_1 in Fe(1 0 0) films, that is discussed below, gives $B_1 = 1$ MJ/m^3 for a 1 nm thin film, which is of opposite sign and different magnitude as compared to the bulk value $B_1^{\text{bulk}} = -3.43$ MJ/m^3. Therefore, it is certainly a severe simplification to discuss the anisotropy in strained nm films under the assumption of bulk magneto-elastic coupling coefficients. Unfortunately, B_2 has not been measured yet in ultrathin epitaxial films, and therefore we cannot present an in-depth discussion of the influence of the modified magneto-elastic coupling on the in-plane anisotropy of nm Fe(1 1 0) films. To demonstrate that modified magneto-elastic coupling coefficients are capable of inducing an in-plane reorientation of the easy axis of magnetization we present in Fig. 1g and Fig. 1h the magneto-elastic anisotropy f_{me} and the sum of $f_{\text{me}} + f_{\text{mc}}$, respectively. We used the experimental value of $B_1 = 1$ MJ/m^3 and set $B_2 = -2$ MJ/m^3. As we do not know of any experimental value for B_2 for a 1 nm thin Fe film under $\approx 1\%$ strain we assumed the same relative change of B_2 versus its bulk value as we measured for B_1. The resulting magneto-elastic anisotropy in Fig. 1g shows an easy magnetization direction along $[\bar{1}\ 1\ 0]$. We plot in Fig. 1h the magneto-elastic anisotropy from Fig. 1g as a dashed curve, and show the bulk magneto-crystalline anisotropy from Fig. 1c as a dotted curve. The resulting sum of both anisotropy contributions is plotted as a solid curve and indicates an easy magnetization direction along $[\bar{1}\ 1\ 0]$. The magnitude of the anisotropy differs from the surface term model, but no attempts were made to mimic these values. Our goal is to demonstrate that the modified magneto-elastic coupling offers a convenient approach to account for the anisotropy of ultrathin epitaxial films without having to invoke surface anisotropy terms a priori.

Clemens et al. [25] pointed out that even an apparent $1/d$ dependence of the crystalline anisotropy of a strained Fe(1 1 0) film does not necessarily require a surface term model $K_1 + K_S/d$ for its explanation. Instead, these authors used a model to describe the in-plane strain as a function of film thickness to mimic a $1/d$ dependence of the magnetic anisotropy as a film thickness dependent magneto-elastic energy contribution [25].

In conclusion, neither a modified in-plane anisotropy in epitaxial films nor an apparent $1/d$ dependence of the magnetic-anisotropy is an unequivocal justification for the so-called surface anisotropy terms. However, it is physically appealing to take the symmetry breaking at surface and interfaces via surface terms into account [18,26–30]. But the decisive role of strain for the modified magnetic anisotropy, as evidenced in experimental investigations and first-principles calculations [31] has to be considered also. An experiment that correlates film strain with magneto-elastic coupling is described next.

3. Magnetostrictive bending of film–substrate composites

Magnetostriction of bulk Fe samples is known as a small relative elongation of order 10^{-5} that can be induced by magnetizing the sample. In ultrathin films however, the ferromagnetic film is rigidly bonded to a substrate, and in the limiting case of an indefinitely rigid substrate, no magnetostrictive strain will be observed: although the magnetization process does induce magneto-elastic stresses in the ferromagnetic film, the indefinitely rigid film–substrate composite does not yield to these stresses. On thin substrates with a thickness of order 100 μm, the magneto-elastic stresses of ferromagnetic films lead to a minute deflection of the film–substrate composite. Thus, monitoring the change of radius of curvature of a film–substrate composite during magnetization processes is a standard tool to examine the magneto-elastic properties of thin films [32–39].

As we are interested in the magneto-elastic properties of monolayer thin epitaxial films, grown on single crystal substrates, we employ a very sensitive optical-deflection technique to measure the minute deflection of a 100 μm thin W(1 0 0) single crystal substrate due to the magnetization of epitaxial Fe films as thin as three atomic layers [10,40]. The resulting radius of curvature of the film–substrate composite is of order 200 km, and phase-sensitive detection schemes are employed to achieve this high sensitivity [41]. A sketch of the optical deflection technique is presented in Fig. 2a. A second set of the deflection technique is used to measure

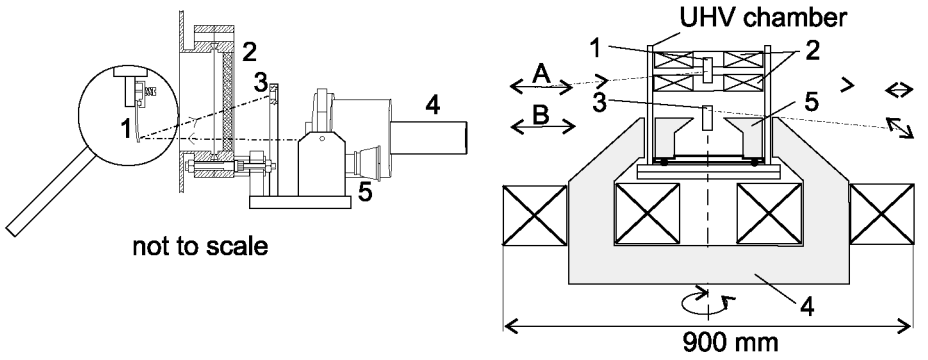

(a) (b)

Fig. 2. (a) Schematic diagram of the optical deflection technique. A laser beam is deflected from the substrate, located inside of the UHV chamber, onto a position-sensitive detector to monitor the curvature of the substrate. 1: single crystal substrate, 2: UHV-window, 3: position-sensitive detector, 4: laser, 5: adjustable laser mount. (b) Cross section through lower part of the UHV chamber with magnet system. 1: sample in a position for transversal MOKE, 2: stainless-steel capsuled, water-cooled electromagnet (vertical fields of up to 0.1 T), 3: sample in the position for longitudinal and polar MOKE and magneto-elastic bending experiments, 4: external electromagnet with 5: internal pole pieces, rotatable around vertical axis (fields of up to 0.4 T). After Ref. [10].

film stress during film growth, as described in Section 4. Electromagnets within the ultra-high vacuum (UHV) chamber, and an external magnet with its pole pieces inside the vacuum chamber are employed to magnetize the film in fields of up to 0.4 T. The magneto-optical Kerr effect (MOKE) is used to monitor the film magnetization in situ. A schematic of the electromagnets at the lower part of our UHV chamber is shown in Fig. 2b.

We employ W(1 0 0) substrates with the [1 0 0] directions oriented along the sample length and width, respectively. From the expression of the magneto-elastic energy density $f_{me} = B_1\varepsilon_1\alpha_1^2 + \cdots$ it follows that a magnetization along the direction 1, along the sample length, induces a magneto-elastic stress τ_1^{me} of

$$\tau_1^{me} = \frac{\partial f_{me}}{\partial \varepsilon_1} = B_1. \tag{16}$$

A negative value of B_1, as found in bulk Fe, induces compressive stress, that tries to strain the film to increase its length. If the magnetization is switched to the direction 2, along the sample width, the magneto-elastic stress is induced along the sample width, and the stress along the sample length changes. We monitor the curvature of the sample along the sample length, and the resulting change of the radius of curvature R_1 gives B_1 [13]:

$$B_1 = \frac{Y_S t_S^2}{6(1+\nu_S)t_F}\left(\left(\frac{1}{R_1}\right)^{length} - \left(\frac{1}{R_1}\right)^{width}\right). \tag{17}$$

$Y_S = 402$ GPa and $\nu_S = 0.28$ are the Young modulus and the Poisson ratio of the W substrate, respectively. For general substrate orientations of elastic anisotropic materials, the directional dependence of the elastic properties has to be considered [13]. The sample thickness is given by t_S, the film thickness is t_F. The superscripts *length* and *width* denote the magnetization direction. We derive the magneto-elastic coupling coefficient B_1 from a measurement of the difference in sample curvature for magnetization along the sample length versus magnetization along the sample width. A derivation of an equivalent expressions in terms of the magnetostriction constants λ and elastic constants c_{ij} based on energy minimization procedures has been presented [42,43]. The application of the optical deflection technique to measure film stress during film growth is presented next.

4. Stress and strain in epitaxial films

The evaluation of the substrate curvature during film growth is a well-known technique to measure stress with sub-monolayer sensitivity [44–50]. The in situ combination of stress measurements during film growth with provisions for film magnetization to study magneto-elastic properties has been demonstrated by Weber et al. to be a powerful tool to correlate mechanical film stress with the magnetic properties of ultrathin Fe films [9]. We used the optical deflection technique to measure the anisotropic film stress of epitaxial Fe monolayers on W(1 1 0) [13,50]. Stress measurements for the growth of Fe on W(1 0 0) are presented in Section 5 where we discuss the important role of film stress for the modified magneto-elastic coupling in these films. In the following we present a brief discussion of stress-driven structural changes in Fe monolayers on W(1 1 0), that has been presented in greater detail elsewhere [13,51].

The strain in pseudomorphic epitaxial films is given by the lattice mismatch between film and substrate, in the case of Fe and W one calculates an isotropic in-plane strain of $\eta = a_W/a_{Fe} - 1 = 0.104$ from the lattice constants $a_W = 3.165$ Å and $a_{Fe} = 2.866$ Å [52]. To derive an estimate of the resulting film stress we apply continuum crystal elasticity and obtain the following stress–strain relations from the elastic energy density $f^{(1\,1\,0)}_{\text{elastic}}$ [13]:

$$f^{(1\,1\,0)}_{\text{elastic}} = \frac{4(c_{11}+c_{12})c_{44}\varepsilon_1'^2 + 8c_{12}c_{44}\varepsilon_1'\varepsilon_2' + (c_{11}^2 - 2c_{12}^2 + c_{11}(c_{12}+2c_{44}))\varepsilon_2'^2}{2(c_{11}+c_{12}+2c_{44})},$$

$$\tau_1' = \frac{\partial f^{(1\,1\,0)}_{\text{elastic}}}{\partial \varepsilon_1'} = \frac{4(c_{11}+c_{12})c_{44}\varepsilon_1' + 4c_{12}c_{44}\varepsilon_2'}{c_{11}+c_{12}+2c_{44}}, \tag{18}$$

$$\tau_2' = \frac{\partial f^{(1\,1\,0)}_{\text{elastic}}}{\partial \varepsilon_2'} = \frac{4c_{12}c_{44}\varepsilon_1' + (c_{11}^2 - 2c_{12}^2 + c_{11}(c_{12}+2c_{44}))\varepsilon_2'}{c_{11}+c_{12}+2c_{44}}. \tag{19}$$

Inserting the values of the isotropic in-plane strain of $\varepsilon_1' = \varepsilon_2' = \eta = 0.1$ and taking the bulk elastic constants from Table 4 reveals that – although the strain is isotropic – the stress is highly anisotropic: the in-plane stress along $[\bar{1}\,1\,0]$, $\tau_1' = 38.9$ GPa, is 41% larger than the in-plane stress along [0 0 1], $\tau_2' = 27.5$ GPa. The elastic energy density of the pseudomorphically strained Fe(1 1 0) film is 3.36 GJ/m^3, which gives a tremendous strain energy per Fe atom of 0.32 eV/atom. Therefore, the reduction of the elastic strain energy is expected to be a dominant driving force for structural transitions. Our stress measurements show that misfit distortions are introduced already in the second layer of Fe, lowering the film stress significantly. As discussed next, the *measured* stress in the pseudomorphic region is 65 GPa along [0 0 1] and 44 GPa along $[\bar{1}\,1\,0]$, respectively. These results indicate a considerable discrepancy between measured film stress and calculated stress. However, the calculated stress anisotropy is also found in the experiments. One should not expect that bulk elasticity applies to the first Fe monolayer, as a bulk-like electronic structure should be a necessary requirement for bulk elastic properties, but photo-electron spectroscopy suggests that at least five layers are needed before a bulk-like electronic structure evolves [53,54]. The impact of electronic surface and interface states on the surface stress and on the elastic properties of the surface layer remains to be investigated.

The calculated in-plane anisotropy of the film stress requires that the radius of curvature of the sample is measured along the in-plane $[\bar{1}\,1\,0]$ (R_1) and [0 0 1] (R_2) directions to calculate the film stresses τ_1 and τ_2:

$$\tau_1 = \frac{Y_S t_S^2}{6(1-\nu_S^2)t_F}\left(\frac{1}{R_1} + \nu_S\frac{1}{R_2}\right),$$

$$\tau_2 = \frac{Y_S t_S^2}{6(1-\nu_S^2)t_F}\left(\frac{1}{R_2} + \nu_S\frac{1}{R_1}\right). \tag{20}$$

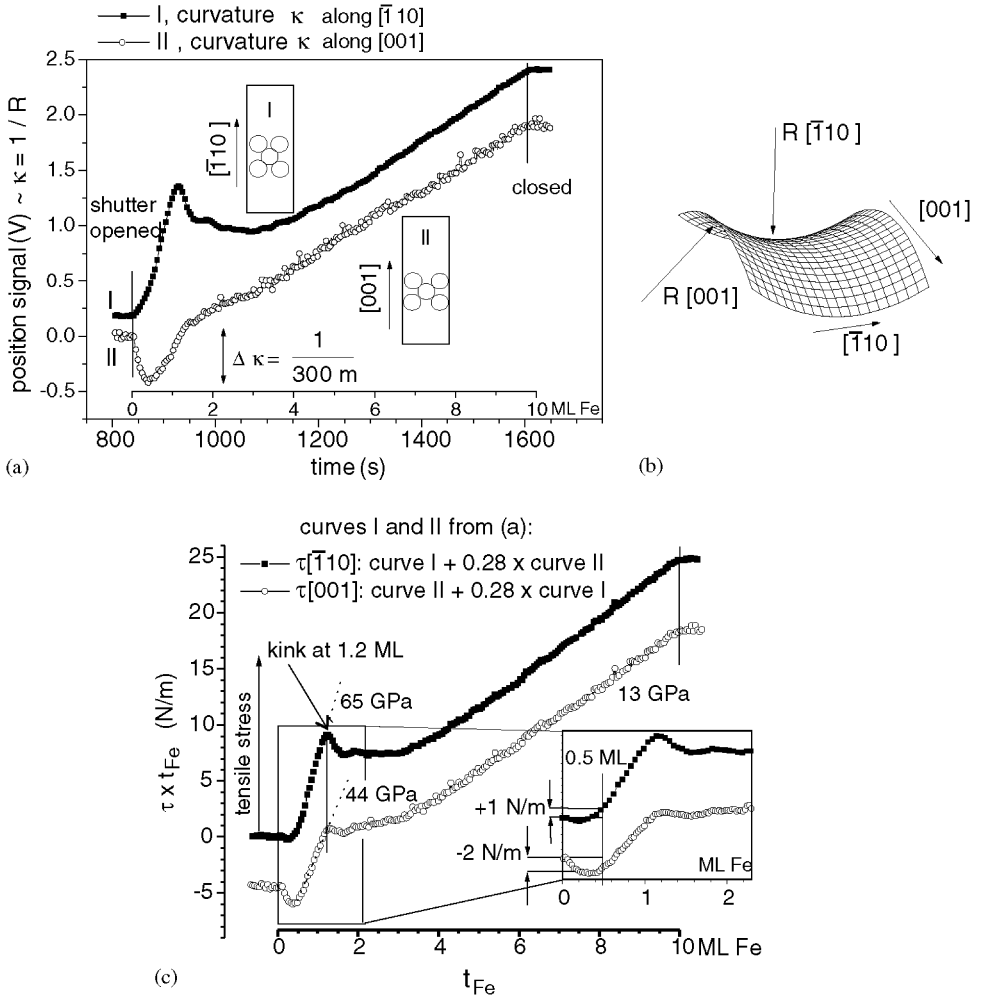

Fig. 3. Biaxial stress analysis for the room-temperature growth of Fe on W(1 1 0). (a) Curvature κ data for two differently oriented crystals. The growth of Fe induces curvatures of opposite sign in the sub-monolayer range, leading to an antielastic substrate curvature shown in (b). (c) The curvature data from (a) are weighed by the Poisson ratio of W and added to arrive at the plots of $\tau_i \times t_{Fe}$ versus t_{Fe}. A positive slope indicates tensile film stress, the kink at 1.2 ML indicates the formation of misfit distortions in the second Fe layer. After Ref. [50].

The curvature analysis is greatly simplified in the case of elastic isotropic substrates as W. The flexural rigidity of the substrate is isotropic and the compact Eq. (20) describes the biaxial stress analysis properly [13].

We measured the substrate curvature during film growth on two differently cut crystals, as shown in Fig. 3. The rectangular crystals were oriented with their length along [$\bar{1}$ 1 0] [upper curve in Fig. 3a] and along [0 0 1] [lower curve in Fig. 3a]. The position signal of the position-sensitive detector shown in Fig. 2a is monitored during the deposition of 10 ML Fe at room temperature. Quite surprisingly, the deposition of Fe induces crystal curvatures of opposite sign along the two directions in the sub-monolayer range. The crystal is bent like the anticlastic surface shown in Fig. 3b. Although diffraction experiments indicate pseudomorphic growth with an isotropic strain in the first Fe layer, the Fe-induced surface forces are of opposite sign. This

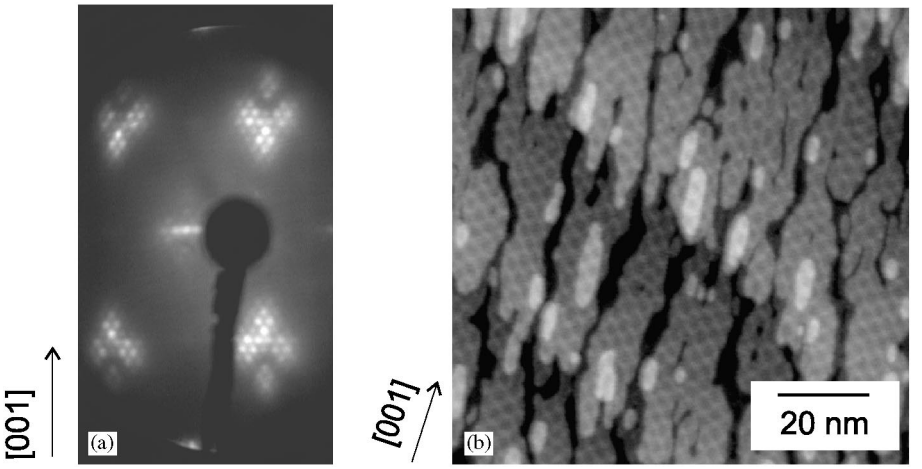

Fig. 4. (a) LEED image of 3 ML Fe on W(1 1 0). Additional diffraction spots are arranged in diamond-shaped areas around the (1 1 0) diffraction spots, indicative of a regular distortion line network. (b) STM image of 3 ML Fe on W(1 1 0). Elongated islands of the third layer are shown in grey, with patches of the fourth layer in lighter grey. Distortion lines are detected as regularly arranged lighter grey lines on top of the Fe islands. From Ref. [51].

result is a clear example for the failure of strain arguments to explain sub-monolayer stress. Instead, the change of surface stress of the clean W surface in comparison to the Fe–W composite is suggested to be responsible for the anisotropic curvature in the sub-monolayer range [50]. With increasing coverage, both curvature data show a positive slope, as expected from the tensile strain in the Fe film. A kink in the curvature data around 1.2 ML indicates the formation of misfit distortions in the film. This leads to slightly decreasing curvature along $[\bar{1}\,1\,0]$ up to 4 ML Fe coverage, whereas the formation of misfit distortions leads to a reduced slope of the curvature along [0 0 1]. The curvature data are weighed with the Poisson ratio of the substrate according to Eq. (20) to derive the biaxial stress analysis in Fig. 3c. The slope of the curves in (c) give the film stress components τ_1 in the upper curve, and τ_2 in the lower curve. The slope in the pseudomorphic range indicates an isotropic film stress of 65 GPa along $[\bar{1}\,1\,0]$ versus 44 GPa along [0 0 1]. The inset shows an enlargement of $\tau \times t_{\mathrm{Fe}}$ on the left scale versus the film thickness in the monolayer range. The anisotropic curvature described above leads to compressive film stress along [0 0 1], although the Fe film is pseudomorphically strained by more than 10%.

Low-energy electron diffraction (LEED) [55] and scanning tunneling microscopy (STM) [56] reveal the atomic structure of the misfit distortions as additional lines of Fe that are first inserted along the [0 0 1] direction in the second layer before a two-dimensional distortion network evolves at higher coverages. LEED and STM images that indicate the two-dimensional distortion line network in a 3 ML thin Fe film are presented in Fig. 4. Additional diffraction spots surrounding the (1 1 0) diffraction spots indicate a high symmetry of the distortion network in the LEED image (a). The distortion line network gives rise to a slight corrugation of the vertical contrast shown in the STM image (b) as lighter grey lines on top of the islands of the third and fourth layer.

In summary, stress measurements are a powerful tool to detect structural transitions with high sensitivity. The resulting changes in film stress can be measured directly. In the case of Fe growth on W(1 1 0), the formation of misfit distortions in the second layer reduces the film stress from more than 40 GPa in the first layer to almost zero in the second and third layer. Tremendous stress variations are expected on a nanoscale where the pseudomorphically strained first layer coexists with stress-relaxed patches of the second layer and

strain-driven variations of the magnetic anisotropy can be expected [47,57]. Unfortunately, the strong in-plane anisotropy of Fe monolayers on W(1 1 0) leads to tremendously high in-plane magnetic fields of order 3.5 T [16] to rotate the magnetization in-plane, as required for a direct measurement of the magneto-elastic coupling. Therefore, we switch in the last section to Fe on W(1 0 0), where the in-plane magnetization rotation can be performed with small magnetic fields.

5. Strain-induced modification of the magneto-elastic coupling

The in situ combination of stress measurements due to epitaxial misfit with stress measurements during magnetization processes is used to investigate the influence of film stress on the magneto-elastic coupling directly. We present results for the room-temperature growth of nm Fe films on W(1 0 0) that indicate that even moderate strains in the sub-percent range induce a significant change of the magneto-elastic coupling coefficient B_1. Our results suggest that even small strains, that are commonly observed in epitaxial films due to the lattice mismatch between film and substrate, invalidate the use of bulk magneto-elastic coupling coefficients.

Film stress is measured during the growth of Fe on W(1 0 0) with the optical deflection technique presented in Fig. 2a. The curvature analysis is simplified for the growth of an (1 0 0) film, as for this orientation, $R_1 = R_2 = R$ in Eq. (20), resulting in the so-called Stoney-equation for a curvature analysis of isotropic stress on elastic isotropic substrates [13]:

$$\tau = \frac{Y_S t_S^2}{6(1-\nu_S)t_F}\left(\frac{1}{R}\right). \tag{21}$$

The biaxial rigidity of the W substrate crystal is given by $Y_S/(1-\nu_S) = 558$ GPa, the substrate thickness is $t_S = 100$ μm, the film thickness is given by t_F.

The relation between isotropic film strain ε_0' and film stress τ_F', as calculated from continuum crystal elasticity is given by [13]

$$\tau_F' = \frac{Y_F}{(1-\nu_F)}\varepsilon_0'. \tag{22}$$

Applying Fe bulk elastic constant gives $Y_F/(1-\nu_F) = 208$ GPa. The misfit strain of 10% leads to a film stress of order 21 GPa. In the following we use this stress–strain relation to convert the measured film stress to film strain. More exactly, one measures the curvature of the film–substrate composite as a function of time during film growth. The Fe evaporator has been checked to deliver constant growth rates, and the curvature plots are plotted versus film thickness t_F in this work. The curvature $1/R$ is proportional to $\tau \times t_F$, therefore, the slope of the measured curvature plots indicate the stress in the growing layer. If a change of the slope of the curvature plot is observed, one has to worry whether the resulting change of the film stress is found exclusively in the growing layers, leaving the stress in the already grown layers unchanged. This interpretation is justified for the kink in the stress measurements of Fe on W(1 1 0), where other techniques [58] corroborated a pseudomorphically strained first layer, even after the formation of misfit distortions in thicker films. In how far this interpretation is justified in nm films remains to be investigated, preferably by surface diffraction techniques to correlate the surface strain with the measured film stress. This is, however, a formidable task, as nm thick films do not show the sharp diffraction patterns known from epitaxial monolayers, and an unequivocal strain information is not expected to be obtained easily. To circumvent the issue of a possible stress relaxation in already deposited layers when a change of slope of the curvature plots is observed, we only considered the change of the substrate curvature between the beginning and the end of the film growth to obtain the *average* film strain. A continuous slope analysis has been discussed by us elsewhere

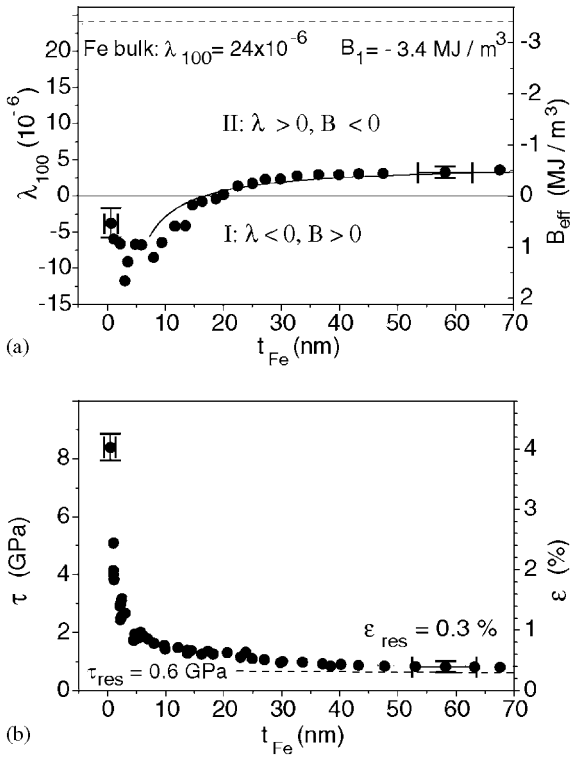

Fig. 5. Measured magneto-elastic coupling B_{eff}, right axis, and calculated $\lambda_{1\,0\,0}$, left axis. The broken line indicates the Fe bulk values. The solid curve describes a strain-dependent correction of B_{eff}, see Fig. 6, calculated from the stress data of (b). (b) Film stress, left axis, and calculated film strain, right axis versus Fe film thickness. From Ref. [8].

[13,24]. However, the main message of this section, that film strain causes B_1 to change in magnitude and sign from its bulk value remains unaffected by the stress averaging technique.

Fig. 5a shows the measured values of the magneto-elastic stress B_1 on the right axis versus the Fe film thickness. On the left axis we present the calculated magnetostriction constant $\lambda_{1\,0\,0}$. In sharp contrast to bulk behavior, the magneto-elastic coupling in Fe films is not constant, but deviates significantly from its bulk value, that is shown as dashed line in Fig. 5a. The apparent thickness variation of B_{eff} leads to reduced magneto-elastic coupling even in the thickest film of 70 nm. B_{eff} shows a zero-crossing around 20 nm and a change of sign for films thinner than 20 nm. That means that Fe films thinner than 20 nm induce tensile stress upon magnetization and try to contract upon magnetization, opposite to what is measured in thicker films.

For each film thickness in (a) we calculate the film stress and the film strain from the curvature measurements performed during film growth. The result is presented in Fig. 5b. The stress is plotted on the left axis, the calculated strain on the right axis. The data points in (b) indicate a rather steep decrease of the film strain with increasing film thickness. In narrow thickness range of only 5 nm, the film stress is reduced from more than 8 GPa ($\varepsilon = 4\%$) to 2 GPa (1%). With increasing Fe thickness, stress and strain approach constant residual values of 0.6 GPa (0.3%). Data for the pseudomorphically strained first monolayers are not included, as the lowest film thickness for the determination of B was 3 atomic layers which is right at the end of the pseudomorphic growth regime, and misfit distortions are being formed and reduce the effective strain.

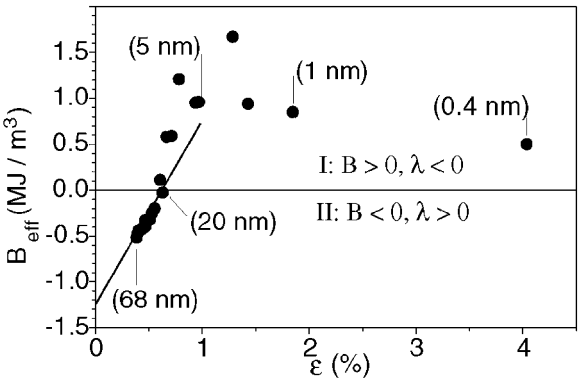

Fig. 6. Effective magneto-elastic coupling B_{eff} versus film strain. The solid curve gives strain-dependent correction of $B_{\mathrm{eff}} = -1.2\ \mathrm{MJ/m^3} + 200\ \mathrm{MJ/m^3}\varepsilon$. After Ref. [8].

To check whether a strain-dependent correction of B_{eff} [5,14]

$$B_{\mathrm{eff}} = B_1 + D\varepsilon \tag{23}$$

is capable of describing the apparent thickness dependence of B_{eff} shown in Fig. 5, we plot in Fig. 6 B_{eff} from Fig. 5a versus ε from Fig. 5b. The solid curve is a fit to the data points in the strain range 0–0.6%. This translates to films thicker than 20 nm. The slope of the curve gives $D = 200 \pm 30\ \mathrm{MJ/m^3}$, the y-intercept gives $B_1 = -1.2 \pm 0.2\ \mathrm{MJ/m^3}$. This strain-dependent correction of B_{eff} describes the experimental data reasonably well in the thickness range 5–68 nm, as indicated by the solid line in Fig. 5a. This simple model breaks down for thinner films, where it predicts huge values of the magneto-elastic coupling coefficients that are *not* observed experimentally. One might speculate that for a film thickness below 5 nm additional surface corrections might contribute via B_S/t_{Fe} [14], leading to an almost constant $B_{\mathrm{eff}} = 1\ \mathrm{MJ/m^3}$ in that thickness range.

The continuous slope analysis of the curvature data obtained during film growth, as described above, leads to different values for the strain-dependent correction of B_{eff}, $B_{\mathrm{eff}} = -3\ \mathrm{MJ/m^3} + 1000\ \mathrm{MJ/m^3}\varepsilon$ [13,24]. These values of $B_1 = -3\ \mathrm{MJ/m^3}$ and $D = 1000\ \mathrm{MJ/m^3}$ agree with the values obtained by Koch et al. on 100 nm thick Fe(1 0 0) films on MgO(1 0 0), that were prepared to be under various stresses of up to 0.8 GPa [5].

The most important message of our investigation is, that in agreement with the work by Koch et al., the magneto-elastic coupling coefficient B_1 is found to deviate in magnitude and sign from its bulk value in strained epitaxial films. Film strain seems to be an important factor for the modified magneto-elastic coupling behavior. Even moderate strains in the sub-percent range are found to induce significant changes of B_1.

6. Conclusion and outlook

Stress measurements with sub-monolayer sensitivity are valuable tools to measure film stress during growth and to investigate the magneto-elastic coupling in ultrathin films directly. The in situ combination of both applications reveals the important role of film strain for the modified magneto-elastic coupling in strained epitaxial films. It is found that in sharp contrast to the bulk behavior, the magneto-elastic coupling constant B_1 of Fe is by no means constant, but changes in magnitude and sign with decreasing film thickness.

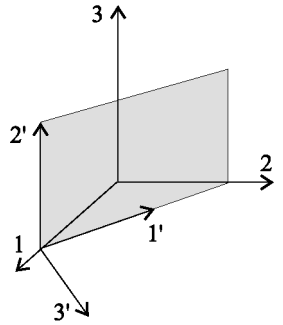

(a)

	1	2	3
1'	$-\frac{1}{\sqrt{2}}$	$\frac{1}{\sqrt{2}}$	0
2'	0	0	1
3'	$\frac{1}{\sqrt{2}}$	$\frac{1}{\sqrt{2}}$	0

(b)

Fig. 7. (a) Sketch of the cubic (1 1 0) plane. The cubic crystal coordinate system is given by the un-primed, the film coordinate system is given by the primed directions. (b) Transformation scheme. Read column by column to obtain crystal coordinates in terms of film coordinates.

A strain-dependent correction of B_1 is found to describe the apparent thickness dependence of B_1 reasonably well for a film thicker than 10 nm. The experimental data suggest that even moderate strains in the sub-percent range are capable of modifying the effective magneto-elastic coupling considerably. The implications of a modified magneto-elastic coupling in nm thin films are profound. *Bulk magneto-elastic constants cannot be expected to apply in the discussion of the magnetic anisotropy of ultrathin films in general.*

Film stress measurements in the sub-monolayer range indicate the diminished importance of strain arguments. Compressive stress, which is of opposite sign as compared to the expectations of strain arguments, is measured for sub-monolayer coverages of Fe on W(1 1 0) along [0 0 1], whereas tensile stress is measured along $[\bar{1}\ 1\ 0]$. The electronic picture of this anisotropic Fe-induced surface stress remains to be elucidated in theoretical calculations.

More experimental work on the direct determination of the magneto-elastic coupling in epitaxial films is clearly called for to check the role of strain-dependent corrections versus the possible contribution of surface corrections. First principles calculation justify the description of the magneto-elastic coupling as the strain derivative of the magnetic anisotropy energy. But no theoretical justification of a strain-dependent correction of the magneto-elastic coupling has been given yet.

Appendix A

The application of anisotropy expressions that are formulated in terms of the un-primed direction cosines and strains of the crystal system requires to express the un-primed variables through the primed variables of the film coordinate system, as indicated in the transformation scheme in Fig. 7. This is done with the following transformation matrix $\boldsymbol{a}$:

$$a_{ij} = \begin{pmatrix} \frac{-1}{\sqrt{2}} & \frac{1}{\sqrt{2}} & 0 \\ 0 & 0 & 1 \\ \frac{1}{\sqrt{2}} & \frac{1}{\sqrt{2}} & 0 \end{pmatrix}. \tag{A.1}$$

The direction cosines α_i transform as

$$\alpha_i = \sum_{j=1}^{3} a_{ji}\alpha'_j, \quad \text{e.g. } \alpha_1 = -\frac{1}{\sqrt{2}}\alpha'_1 + 0 + \frac{1}{\sqrt{2}}\alpha'_3. \tag{A.2}$$

The transformation of the strains ε_{ij} is most easily done by matrix multiplication, using the transpose of $\boldsymbol{a}$, $\boldsymbol{a}^{\mathrm{T}}$:

$$\varepsilon = \boldsymbol{a}^{\mathrm{T}}\varepsilon'\boldsymbol{a},$$

$$\varepsilon_{ij} = \begin{pmatrix} \frac{1}{2}(\varepsilon'_1 + \varepsilon'_3) & \frac{1}{2}(-\varepsilon'_1 + \varepsilon'_3) & 0 \\ \frac{1}{2}(-\varepsilon'_1 + \varepsilon'_3) & \frac{1}{2}(\varepsilon'_1 + \varepsilon'_3) & 0 \\ 0 & 0 & \varepsilon'_2 \end{pmatrix}. \tag{A.3}$$

References

[1] S. Sun, R. O'Handley, Phys. Rev. Lett. 66 (1991) 2798.
[2] H. Szymczak, R. Żuberek, Acta Phys. Pol. A 83 (1993) 651.
[3] A. Siemko, H. Lachowicz, J. Magn. Magn. Mater. 66 (1987) 31.
[4] J. Barandiarán et al., Phys. Rev. B 35 (1987) 5066.
[5] R. Koch, M. Weber, K. Rieder, J. Magn. Magn. Mater. 159 (1996) L11.
[6] Y. Kim, T. Silva, Appl. Phys. Lett. 68 (1996) 2885.
[7] C. Kittel, Rev. Mod. Phys. 21 (1949) 541.
[8] D. Sander, A. Enders, J. Kirschner, J. Magn. Magn. Mater. 198–199 (1999) 519.
[9] M. Weber, R. Koch, K. Rieder, Phys. Rev. Lett. 73 (1994) 1166.
[10] D. Sander et al., J. Phys. D 31 (1998) 663.
[11] P. Bruno, Magnetismus von Festkörpern und Grenzflächen, Physical origins and theoretical models of magnetic anisotropy, Forschungszentrum Jülich, Jülich, 1993, pp. 24.1–24.28.
[12] J.F. Nye, Physical Properties of Crystals, Oxford University Press, Oxford, 1985.
[13] D. Sander, Rep. Prog. Phys. 62 (1999) 809.
[14] R. O'Handley, S. Sun, J. Magn. Magn. Mater. 104–107 (1992) 1717.
[15] U. Gradmann, J. Korecki, G. Waller, Appl. Phys. A 39 (1986) 101.
[16] H. Elmers, U. Gradmann, Appl. Phys. A 51 (1990) 255.
[17] O. Song, C. Ballentine, R. O'Handley, Appl. Phys. Lett. 64 (1994) 2593.
[18] T. de Lacheisserie, O. McGrath, J. Magn. Magn. Mater. 147 (1995) 160.
[19] M. Stearns, Magnetic properties of 3d, 4d and 5d elements, alloys and compounds, Landolt-Börnstein Numerical Data and Functional Relationships in Science and Technology Group III, Vol. 19a, Springer, Berlin, 1986.
[20] P. Bruno, J. Phys. F 18 (1988) 1291.
[21] F. Jona, P. Marcus, Surf. Rev. Lett. 4 (1997) 817.
[22] R.F.S. Hearmon, The elastic constants of non-piezoelectric crystals, Landolt-Börnstein Numerical Data and Functional Relationships in Science and Technology Group III, Vol. 2, Springer, Berlin, 1969.
[23] R.F.S. Hearmon, The elastic constants of crystals and other anisotropic materials, Landolt-Börnstein Numerical Data and Functional Relationships in Science and Technology Group III, Vol. 18, Springer, Berlin, 1984.
[24] A. Enders, D. Sander, J. Kirschner, J. Appl. Phys. 85 (1999) 5279.
[25] B. Clemens, R. White, W. Nix, J. Bain, Mater. Res. Soc. 231 (1992) 459.
[26] R. Victora, J. MacLaren, Phys. Rev. B 47 (1993) 11583.
[27] G. Bochi, O. Song, R. O'Handley, Phys. Rev. B 50 (1994) 2043.
[28] G. Bochi, C. Ballentine, H. Inglefield, C. Thompson, R. O'Handley, Phys. Rev. B 53 (1996) R1729.
[29] D. Givord, O. McGrath, C. Meyer, J. Rothman, J. Magn. Magn. Mater. 157/158 (1996) 245.
[30] A. Shick, D. Novikov, A. Freeman, Phys. Rev. B 56 (1997) R14259.
[31] M. Kim, L. Zhong, A. Freeman, Phys. Rev. B 57 (1998) 5271.
[32] E. Klokholm, IEEE Trans. Magn. MAG-12 (1976) 819.
[33] A. Itoh, H. Uekusa, Y. Tarusawa, F. Inoue, K. Kawanishi, J. Magn. Magn. Mater. 35 (1983) 241.
[34] A. Tam, H. Schroeder, IEEE Trans. Magn. 25 (1989) 2629.
[35] H. Awano, Y. Suzuki, T. Katayama, A. Itoh, IEEE Trans. Magn. 26 (1990) 2742.
[36] R. Koch, M. Weber, E.A.R.K. Henze, Surf. Sci. 331–333 (1995) 1398.
[37] M. Ciria et al., Phys. Rev. Lett. 75 (1995) 1634.
[38] R. Watts, M.R.J. Gibbs, W.J. Karl, H. Szymczak, Appl. Phys. Lett. 70 (1997) 2607.
[39] A. Hernando, A. Neuweiler, P. Farber, H. Kronmüller, Phys. Rev. B 57 (1998) 7458.
[40] D. Sander, A. Enders, J. Kirschner, IEEE Trans. Magn. 34 (1998) 2015.

[41] A. Enders, Mechanische Spannungen und Ferromagnetismus ultradünner Schichten, Ph. D. Thesis, Martin-Luther Universität Halle-Wittenberg, Mathematisch-Naturwissenschaftlich-Technische Fakultät, 1999.
[42] E. Trémolet de Lacheisserie, J. Peuzin, J. Magn. Magn. Mater. 136 (1994) 189.
[43] P. Marcus, J. Magn. Magn. Mater. 168 (1997) 18.
[44] A. Schell-Sorokin, R. Tromp, Phys. Rev. Lett. 64 (1990) 1039.
[45] R. Koch, J. Phys.: Condens. Matter 6 (1994) 9519.
[46] A. Grossmann, W. Erley, J.B. Hannon, H. Ibach, Phys. Rev. Lett. 77 (1996) 127.
[47] D. Sander, R. Skomski, C. Schmidthals, A. Enders, J. Kirschner, Phys. Rev. Lett. 77 (1996) 2566.
[48] H. Ibach, Surf. Sci. Rep. 29 (1997) 193.
[49] J. Floro et al., J. Electronic Mat. 26 (1997) 969.
[50] D. Sander, A. Enders, J. Kirschner, Europhys. Lett. 45 (1999) 208.
[51] D. Sander, A. Enders, C. Schmidthals, D. Reuter, J. Kirschner, Surf. Sci. 402–404 (1998) 351.
[52] J. Donnay, H. Ondik (Eds.), Crystal Data, National Bureau of Standards, Gaithersburg, MD, 1973.
[53] K. Kämper, W. Schmitt, G. Güntherodt, H. Kuhlenbeck, Phys. Rev. B 38 (1988) 9451.
[54] K. Kämper, W. Schmitt, D. Wesner, G. Güntherodt, Appl. Phys. A 49 (1989) 573.
[55] U. Gradmann, G. Waller, Surf. Sci. 116 (1982) 539.
[56] H. Bethge, D. Heuer, C. Jensen, K. Reshöft, U. Köhler, Surf. Sci. 331–333 (1995) 878.
[57] N. Weber, K. Wagner, H. Elmers, J. Hauschild, U. Gradmann, Phys. Rev. B 55 (1997) 14121.
[58] M. Przybylski, I. Kaufmann, U. Gradmann, Phys. Rev. B 40 (1989) 8631.